Carter *et al. Progress in Earth and Planetary Science* (2018) 5:10
DOI 10.1186/s40645-018-0164-y

Progress in Earth and Planetary Science

RESEARCH ARTICLE Open Access

Unseasonal development of post-sunset F-region irregularities over Southeast Asia on 28 July 2014: 1. Forcing from above?

Brett A. Carter[1*], S. Tulasi Ram[2], Endawoke Yizengaw[3], Rezy Pradipta[3], John Retterer[3], Robert Norman[1], Julie Currie[1], Keith Groves[3], Ronald Caton[4], Michael Terkildsen[5], Tatsuhiro Yokoyama[6] and Kefei Zhang[1]

Abstract

This contribution is the first of a two-part investigation into an unseasonal post-sunset equatorial F-region irregularity (EFI) event over the Southeast Asian region on the evening of 28 July 2014. Ground-based GPS scintillation data, space-based GPS radio occultation (RO) data, and ionosonde data show the existence of EFIs shortly after sunset over a region spanning 30° in longitude and 40° in latitude, centered on the geomagnetic equator. This post-sunset EFI event was observed during a time of the year when post-sunset equatorial plasma bubbles (EPBs) are very infrequent in the Southeast Asian longitude sector. GPS RO data shows that the EFI event over Southeast Asia coincided with the suppression of peak-season EPBs in the African and Pacific longitude sectors. Ionosonde data shows the presence of a strong pre-reversal enhancement (PRE) in the upward plasma drift over Southeast Asia prior to the detection of EFIs. Further, it is reported that this PRE was significantly stronger than on any other day of July 2014. An analysis of the geophysical conditions during this event reveals that this enhanced PRE was not caused by disturbed geomagnetic activity. Therefore, it is hypothesized that forcing from lower altitudes, perhaps tidal/planetary waves, was the potential cause of this strong PRE, and the subsequent EPB/EFI activity, on this day over the Southeast Asian sector.

Keywords: Equatorial plasma bubbles, GPS scintillations, Ionosphere

Introduction

Equatorial plasma bubbles (EPBs) are common nighttime features in the low-latitude ionosphere. After sunset, the bottom of the F layer becomes unstable to the generalized Rayleigh-Taylor (R-T) plasma instability, and low-density plasma bubbles rise up into the high-density ionospheric plasma at higher altitudes (e.g., Kelley et al. 2011). These EPBs generate a wide spectrum of plasma waves/irregularities, called "equatorial F-region irregularities" (EFIs), that interfere with radio signals that propagate through them, such as those used in satellite communications and Global Navigation Satellite Systems (e.g., the Global Positioning System (GPS)). In the presence of EPBs/EFIs, radio signals used by these systems experience random fluctuations in amplitude and phase, termed "ionospheric scintillation," which degrades the quality of the received signal and can even cause a complete loss-of-lock (e.g., Pi et al. 1997; Xiong et al. 2016). Scintillation events are thus detrimental to the applications that rely on these signals, and consequently, researchers have focused efforts towards better understanding EPB events for the purpose of prediction (e.g., Anderson et al. 2004; Retterer 2005; Retterer et al. 2005; Kelley and Retterer 2008; Redmon et al. 2010; Carter et al. 2014c; Anderson and Redmon 2017).

The physical mechanism responsible for the growth of post-sunset EPBs is understood to be the generalized R-T plasma instability, in which the vertical density gradient in the bottomside F layer combines with the pre-reversal enhancement (PRE) in the upward plasma drift to destabilize the plasma after sunset (Sultan 1996 and references therein). Research efforts have been subsequently directed towards explaining why post-sunset EPBs form during some periods, but not others. EPB occurrence variability can be split into two categories: (1)

*Correspondence: brett.carter@rmit.edu.au
[1]SPACE Research Centre, RMIT University, Melbourne, Victoria, Australia
Full list of author information is available at the end of the article

long-term (i.e., seasonal/longitudinal) climatology and (2) short-term (i.e., day-to-day) variability.

The long-term climatology is well understood to be governed by the strength of the PRE, which varies as a function of longitude and season (e.g., Abdu et al. 1981; Tsunoda 1985; Burke et al. 2004). Times of the year when the local magnetic field lines closely align with the day-night terminator exhibit stronger PREs compared to times when they do not align. The PRE strength is partially controlled by the longitudinal E-region conductivity gradient; the stronger the gradient, the stronger the PRE. During seasons when the angle between the magnetic field and the terminator is large, E-region plasma from the dayside leaks onto the nightside via the field lines, thereby reducing the longitudinal conductivity gradient (Abdu et al. 1981; Tsunoda 1985). Statistical studies of both the occurrence of post-sunset EPBs and the PRE strength have been carried out, and the observational evidence appears to support this explanation rather well (e.g., Aarons 1993; Huang et al. 2002; Burke et al. 2004; Nishioka et al. 2008). Further, the post-sunset EPB occurrence climatology reported in satellite data has been well replicated using global ionosphere modeling (e.g., Retterer and Gentile 2009).

The post-sunset EPB occurrence climatology can be conveniently separated into "peak," "transitional," and "off-peak" seasons (e.g., Carter et al. 2014c), the timing of which depends on longitude/magnetic declination. For example, in the Southeast Asian longitude sector, post-sunset EPBs are most common during the equinoctial months and are rare during the solstices (e.g., Burke et al. 2004; Nishioka et al. 2008; Carter et al. 2013). However, high-solar activity conditions can cause comparatively high EPB occurrence in the Asian sector during June solstice months (e.g., Nishioka et al. 2008; Li et al. 2011; Carter et al. 2013). During low solar activity conditions, June solstice post-sunset EPBs in the Asian sector are rare, but their post-midnight counterparts can be rather common (e.g., Yokoyama et al. 2011). As such, solar activity and the local time of the EPB occurrence should also be considered when defining these EPB "seasons."

While the PRE is a dominant term within the R-T plasma instability growth rate and can therefore explain much of the observed post-sunset EPB climatology, it is not the only factor that can lead to EPB generation. For example, Communication/Navigation Outage Forecasting System (C/NOFS) satellite observations reported by Huang and Hairston (2015) showed that EPBs can be present under weak, and even negative, upward plasma drift conditions. C/NOFS observations during the 2008–2009 solar minimum that were reported by Dao et al. (2011) showed convincing evidence that lower atmospheric forcing might play a significant role in EPB generation. In addition to these observations, modeling has shown that R-T growth is still possible under small/negative upward plasma drift conditions (Carter et al. 2016) and that EPB development and characteristics can be significantly influenced by the presence of atmospheric gravity waves (Retterer and Roddy 2014).

The daily variability in EPB occurrence has been more difficult to understand for a number of reasons. First, the daily variability is effectively "superimposed" on top of the background occurrence climatology. EPBs that form during a peak EPB season do not necessarily contribute towards "daily variability" because the conditions were already favorable for their growth. Similarly, a lack of EPBs during off-peak season are not evidence of daily variability. Instead, a lack of EPBs during peak EPB season, and the presence of EPBs during an off-peak season, are core contributors towards daily variability.

A series of recent works have examined the daily EPB occurrence during peak EPB season with the use of the Thermosphere Ionosphere Electrodynamics General Circulation Model (Carter et al. 2014a; b; c). In these works, the daily variability during peak season was captured by the identification of evenings with decreased EPB growth conditions. Further analysis found that relatively small changes in the geomagnetic activity forcing were the cause of daily changes in the EPB growth conditions, via changes in the zonal neutral winds and the PRE at the equator, i.e., a low-magnitude disturbance dynamo effect. However, this technique failed to explain the presence of EPBs during the transitional and off-peak seasons.

Collectively, these previous studies clearly show that the occurrence of unseasonal EPBs is not a new phenomenon. However, understanding all of the physical mechanisms behind the generation of unseasonal EPBs through diagnostic analyses is a necessity in building an accurate EPB prediction capability. As a step towards achieving this goal, one of the unseasonal EPB events uncovered by Carter et al. (2014c) is the focus of the current analysis. In this two-part investigation, the presence of EPBs/EFIs over Southeast Asia during the off-peak EPB season of July 2014 is shown using multiple independent datasets, and the cause of these EPBs is investigated. In this paper, the strength of the PRE in ionosonde data is examined, and the potential influence of the geophysical activity (i.e., "forcing from above") is explored. The second paper in this investigation by Ajith et al. (2017) examines the potential influence of the lower atmosphere in causing this unseasonal EPB event over Southeast Asia (i.e., "forcing from below").

Results

In this investigation, data from the three Southeast Asian GPS stations in the Scintillation Network Decision Aid (SCINDA) network were used (Groves et al. 1997); Bangkok (BKK) in Thailand (100.61 °E, 14.08 °N, magnetic

latitude (MLAT): 6.18 °N), Bandung (BNG) in Indonesia (107.59 °E, 6.89 °S, MLAT: 16.48 °S), and Calcutta (CAL) in India (88.37 °E, 22.58 °N, MLAT: 15.57 °N). The SCINDA GPS receivers monitor the level of ionospheric scintillation using the amplitude scintillation S4 index. The presence of ionospheric scintillation events was indicated by the 90th percentile of the hourly S4 measurements from all satellite-to-ground links. In order to avoid contamination from multipath effects, only S4 data from satellites more than 30° above the horizon were considered. The analysis of GPS scintillation data is augmented by the two SCINDA VHF scintillation stations: Kwajalein Atoll (KWA) in the Marshall Islands in the Pacific sector (167.47 °E, 9.40 °N, MLAT: 4.32 °N) and Bahir Dah (BHD) in Ethiopia in the African sector (37.40 °E, 11.57 °N, MLAT: 2.61 °N).

GPS radio occultation (RO) data from the FORMOSAT-3/Constellation Observing System for Meteorology, Ionosphere and Climate (COSMIC) satellites (Rocken et al. 2000; Anthes 2011) were also used in this study. The GPS RO ionospheric electron density profiles (i.e., "ionPrf") and the ionospheric scintillation profiles (i.e., "scnLv1") collected from all over the world by the COSMIC satellites were used. It should be noted that the electron density profile product is a "level 2" product, whereas the scintillation profile is a "level 1b" product. As such, quality control procedures can tend to cause differences in the number of RO profiles published at each product level; i.e., the number of electron density profiles is typically less than or equal to the number of scintillation profiles.

Finally, ionosonde data from the Global Ionospheric Radio Observatory (GIRO) (Reinisch and Galkin 2011) station at Sanya, China (109.42 °E, 18.34 °N) and the SouthEast Asia Low-latitude IOnospheric Network (SEALION) (Maruyama et al. 2007) station at Bac Lieu (BCL), Vietnam (105.71 °E, 9.3 °N) were used.

Figure 1 shows the hourly 90th percentile of the S4 index measured by the BKK (a), BNG (b), and CAL (c) GPS ground stations as a function of local time (LT) throughout the month of July 2014. It can be seen that the scintillation levels were low all month, with the exception of 28 July, when the scintillation level increased across all three stations from 19–20 LT until close to midnight. This event is also noticeable in the analysis by Carter et al. (2014c) (see the top 3 panels of their Fig. 2). While the scintillation level increase was substantially smaller for the BKK station compared to the others, it is still noticeable. The GPS S4 values scale linearly with the background electron density (Whalen et al. 2009). Therefore, the lower S4 values measured by BKK compared to the other stations can be understood in terms of the lower background electron density expected above the BKK station, which is located beneath the equatorial ionization anomaly trough. The use of ground-based GPS S4 data to indicate the presence/absence of EPBs can be difficult and unreliable in such circumstances and does not allow a simple S4 threshold to be employed. Therefore, it is important to use corroborating data from different sources in order to be certain that EPBs were present.

To supplement the ground-based GPS scintillation observations, we incorporate the global RO ionospheric scintillation observations collected by the COSMIC satellites. Figure 2 shows the locations of the GPS RO event tangent points for which the maximum scintillation levels (i.e., "S4max9sec") were greater than 0.3 between the altitudes of 150 and 400 km in the post-sunset hours (i.e., 19–00 LT) during 27–29 July 2014; the remaining post-sunset RO events are shown in gray. This GPS RO scintillation threshold and these altitude boundaries have been shown to be quite effective in isolating scintillation events caused by EFIs in the post-sunset F layer (e.g., Carter et al. 2013; Yu et al. 2017). Note that the tangent points between the altitudes of 80 and 600 km are plotted. The locations of the GPS ground stations (diamonds) and ionosondes (crosses) used in this analysis are also shown for reference.

Before interpreting the RO scintillation maps, it is important to remember that the tangent point locations shown in Fig. 2 may not represent the actual location of the ionospheric irregularities and could be inaccurate on the order of 10° (Dymond 2012). In the top panel of Fig. 2, the RO scintillation events on 27 July 2017 occurred predominantly over Africa and the Pacific Ocean, with a noticeable lack of scintillation over Southeast Asia and South America. These results are quite similar to those in the bottom panel, which shows the locations of RO scintillation events detected on 29 July 2014, although on 29 July, the RO scintillation locations were observed a little further to the west of the Pacific Ocean towards East Asia. This pattern is rather consistent for other days throughout late July that are not shown here. Further, the locations of these scintillation events are consistent with the background climatology of the global EFI occurrence for the June solstice months reported by Carter et al. (2013) (see their Fig. 5) and Burke et al. (2004) (see their Fig. 1); post-sunset EPBs are commonly detected over the African and Pacific longitude sectors during this time of year. The scintillation events observed on 28 July 2014 (middle panel), on the other hand, show significant scintillation activity above Southeast Asia and nowhere else around the world. The region over which GPS scintillations were detected on 28 July spans almost 30° in longitude from India to China/Indonesia and approximately 40° in latitude centered on the magnetic equator (~ 10 °N).

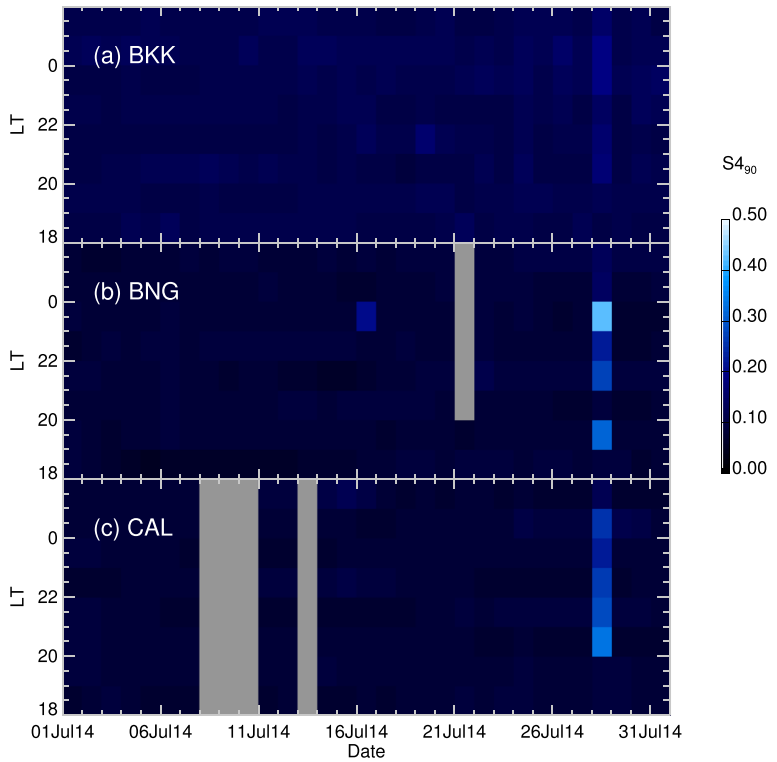

Fig. 1 The 90th percentile of the hourly S4 index S_{90} as a function of local time and date throughout July 2014, as detected by **a** BKK, **b** BNG, and **c** CAL GPS stations. Gray cells indicate data gaps

While the GPS scintillation detection patterns in the RO data appear to agree well with the well-known post-sunset EPB climatology and the ground-based GPS data in Fig. 1, the supporting VHF scintillation data should also be analyzed. Figure 3 shows the VHF amplitude scintillation index S4 measured by the SCINDA KWA (Pacific sector) and BHD (African sector) stations over the 27–29 July 2014 period. The yellow shaded areas indicate the local times between ∼19 and 02 LT, i.e., the post-sunset sector when GPS scintillation is typically observed. The lack of GPS RO post-sunset scintillation observed on 28 July in Fig. 2 is confirmed by both Pacific and African stations in Fig. 3. Notably, BHD shows the presence of late scintillations on 28 July that could either be evidence of local post-midnight EPB growth or non-local post-sunset EPBs that have drifted over Africa from the east. Although, it is clear from the BHD data that post-sunset growth conditions were suppressed on 28 July compared to the days before and after.

The red rectangle in Fig. 2 that highlights the scintillating RO events over Southeast Asia on 28 July 2014 is focused upon in a 3-dimensional format in Fig. 4. Plotted in the left and right columns are the ionospheric scintillation and electron density profiles provided by COSMIC, respectively, each hour from 11 until 15 UT on 28 July 2014. Projections of these RO profiles are given in the latitude-longitude plane at 0 km altitude, along with the ground stations' locations shown in Fig. 2 for reference. In addition, the altitudes of the peak electron density, as determined from each RO event, are shown as black dashes for each profile in the longitude = 70° plane in the right column.

First, during 11–12 UT (i.e., Fig. 4a, b), the scintillation levels were low at F-region altitudes with some RO profiles showing a elevated scintillation at ∼100 km altitude (i.e., the E-region). The scintillation enhancements at 100 km altitude are clear signatures of sporadic E layers, as shown by previous works (Wu et al. 2005; Arras et al. 2008; Brahmanandam et al. 2012; Chu et al. 2014). The corresponding electron density profiles nicely show the well-known higher ionospheric peak altitudes in the equatorial region with a decline in altitude away from the magnetic equator, i.e., the so-called "fountain effect."

In the next hour, 12–13 UT, the RO scintillation profiles show elevated scintillation at F-region altitudes directly above the BCL ionosonde station and the BKK GPS station (approximately the center of the plot). There were two other RO events during this hour that exhibited increased F-region scintillation activity; one of those soundings appears to have ceased prematurely due to the scintillation

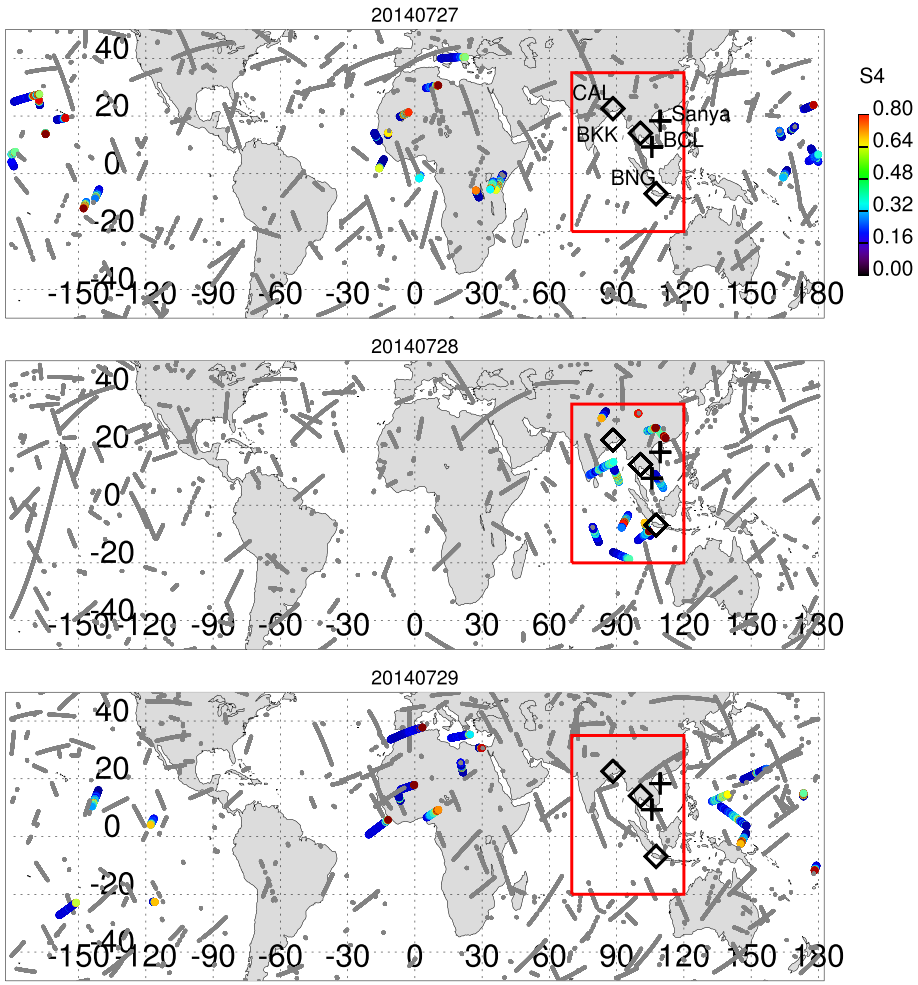

Fig. 2 Global maps showing the locations of COSMIC RO events for which the detected scintillation level "S4max9sec" exceeded 0.3 at F-region altitudes (150–400 km) during the post-sunset hours (i.e., 19–00 LT) of 27 July 2014 (top panel), 28 July 2014, (middle panel), and 29 July 2014 (bottom panel). Also shown are the locations of the SCINDA GPS stations (diamonds) and the Sanya and BCL ionosondes (crosses). The gray points show post-sunset COSMIC RO events with scintillation levels that did not exceed 0.3 at F-region altitudes. The red rectangle highlights the Southeast Asian sector that is analyzed further in Fig. 4

activity and then restarted at a lower altitude (to the south of the BCL station). In Fig. 4d, there are only two corresponding electron density profiles, which indicate that the quality control procedure has excluded the third "broken" profile in Fig. 4c, possibly due to the increased scintillation levels. Interestingly, the altitudes that correspond to high scintillation levels tend to correspond to low-electron densities within the RO profiles, in particular, the RO event over the BCL and BKK stations.

During 13–14 UT, there is a lower number of RO events across the region of interest, but the RO event that occurred close to the geographic equator shows increased scintillation levels, and once again exhibits the corresponding lower electron densities noted above. The decreased number of electron density profiles compared to the scintillation profiles is also evident during 14–15 UT in Fig. 4g-h; only two profiles out of six appear to have passed quality control. The profile in the center of these plots shows increased scintillation activity in the topside ionosphere, whereas the southernmost profile shows scintillations below the F-layer peak with low background electron densities, similar to those noted above. F-region scintillation activity continues in the GPS RO dataset until 21 UT, not shown here, with results consistent with the 11–15 UT data.

The Sanya and BCL ionosondes collected data in the same region as the GPS ground stations and COSMIC RO soundings during this period and are thus used to complement the data presented above. Figure 5 shows a range-time-intensity-style plot of the ionospheric echoes measured by the Sanya ionosonde during 27–29 July 2014. The cells are colored according to the number of echoes

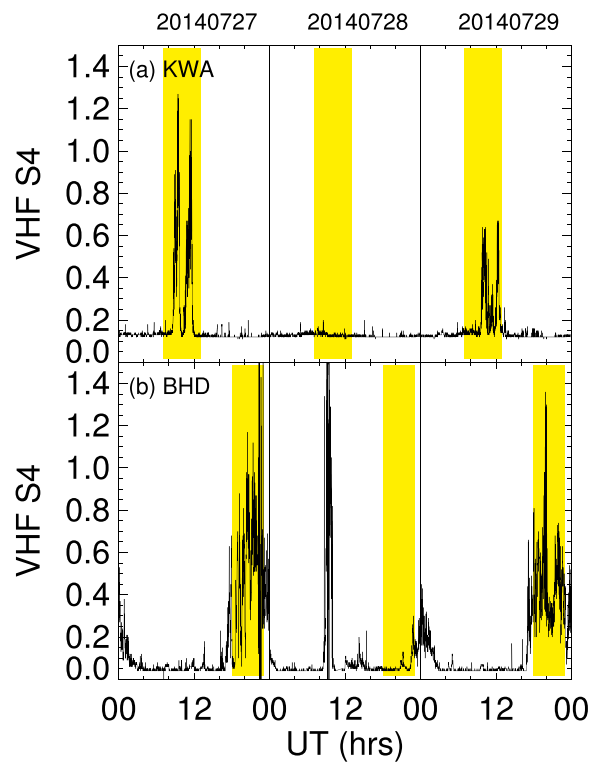

Fig. 3 VHF S4 index measured by the KWA (**a**) and BHD (**b**) ground stations during 27–29 July 2014. The yellow shaded areas indicate 19–02 local time

detected across all sounding frequencies every 15 min. Note that LT $\simeq$ UT + 7, so post-sunset begins close to 12 UT.

Figure 5 shows significant spread F activity after 12 UT on 28 July 2014, and no spread F activity on the day prior or the day after. The commencement of spread F activity on 28 July 2014 is shrouded by blanketing sporadic E, which is consistent with the GPS RO profiles that occurred above the Sanya station in Fig. 4a. The blanketing sporadic E prevents the reception of echoes from the F layer during the initiation of spread F, and as such, the PRE cannot be tracked from this station. Once the sporadic E disappears, the range of virtual heights covered by the spread F is approximately 300–500 km, which is also largely consistent with the GPS RO observations of scintillation activity in Fig. 4.

Figure 6 shows the h'F variation measured by the BCL ionosonde from the late-afternoon sector until the early morning for the entire month of July 2014 (dots). The hourly average of the h'F variation across the month is shown by the black line, and the error bars represent the standard deviation. The yellow, red, and blue curves show the h'F variation on 27, 28, and 29 July 2014, respectively, and the horizontal bar indicates the presence of equatorial spread F (i.e., EFIs) on 28 July.

It is clear from Fig. 6 that the F layer rose to a much higher altitude on 28 July 2014 compared to the rest of the month. In addition, the speed of this ascent (i.e., the PRE) on 28 July was 31.6 m/s, compared to the monthly average 6.4 m/s (i.e., $\sim$ 5 times the monthly average). Following the F layer rise, EFIs were present above the BCL station from 20 LT until dawn the next day.

Discussion

Presented in this study is an ionospheric scintillation event that was detected by GPS receivers across Southeast Asia on the evening of 28 July 2014. The same event was captured as enhanced scintillation activity by coincident GPS RO soundings and spread F by two Southeast Asian ionosondes. The agreement between these independent observations, and the different observation techniques, provides assurance that the ionospheric scintillation event detected on this evening was caused by EPBs via the R-T plasma instability.

In this longitude sector, EPBs are most common during the equinox months and rare during the solstices. Under high-solar activity conditions, EPBs have been commonly observed in the Southeast Asian longitude sector close to the June solstice (see 2002 data in Li et al. (2011)'s Fig. 3). While 2014 was technically a solar maximum year, the F10.7 solar flux during the second half of July 2014 was rather low, an average of 113 solar flux units (s.f.u.) compared to 153 s.f.u. in June 2002. Therefore, this event on 28 July 2014 can be classified as an unseasonal post-sunset EPB event.

As explained earlier in the "Introduction" section, recent research has indicated that the driving factors in the daily variability of EPBs are dependent upon the underlying seasonal conditions (e.g., Carter et al. 2014c). That is, during seasons that provide favorable EPB growth conditions, the daily variability in EPB occurrence is controlled by the days for which EPBs are suppressed. Similarly, for the seasons during which EPB growth is not favorable, the daily variability is controlled by the days for which the growth of EPBs is abnormally enhanced. The event studied here falls under the category of the latter, i.e., an unusual night of EPB growth during an off-peak EPB season. Therefore, the EPB event on 28 July 2014 must be explained in terms of a physical mechanism that has provided enhanced EPB growth conditions.

It is well known that the PRE strength is an important parameter in controlling the growth of EPBs (e.g., Abdu et al. 1981; Tulasi Ram et al. 2006; Su et al. 2008; Carter et al. 2014a) and that the PRE itself can exhibit a strong daily variability (e.g., Scherliess and Fejer 1999). Figure 6 showed that the plasma above the BCL ionosonde rose significantly faster on the evening of 28 July compared to the rest of the month. This suggests that the growth of EPBs on the evening of 28 July 2014 can be attributed

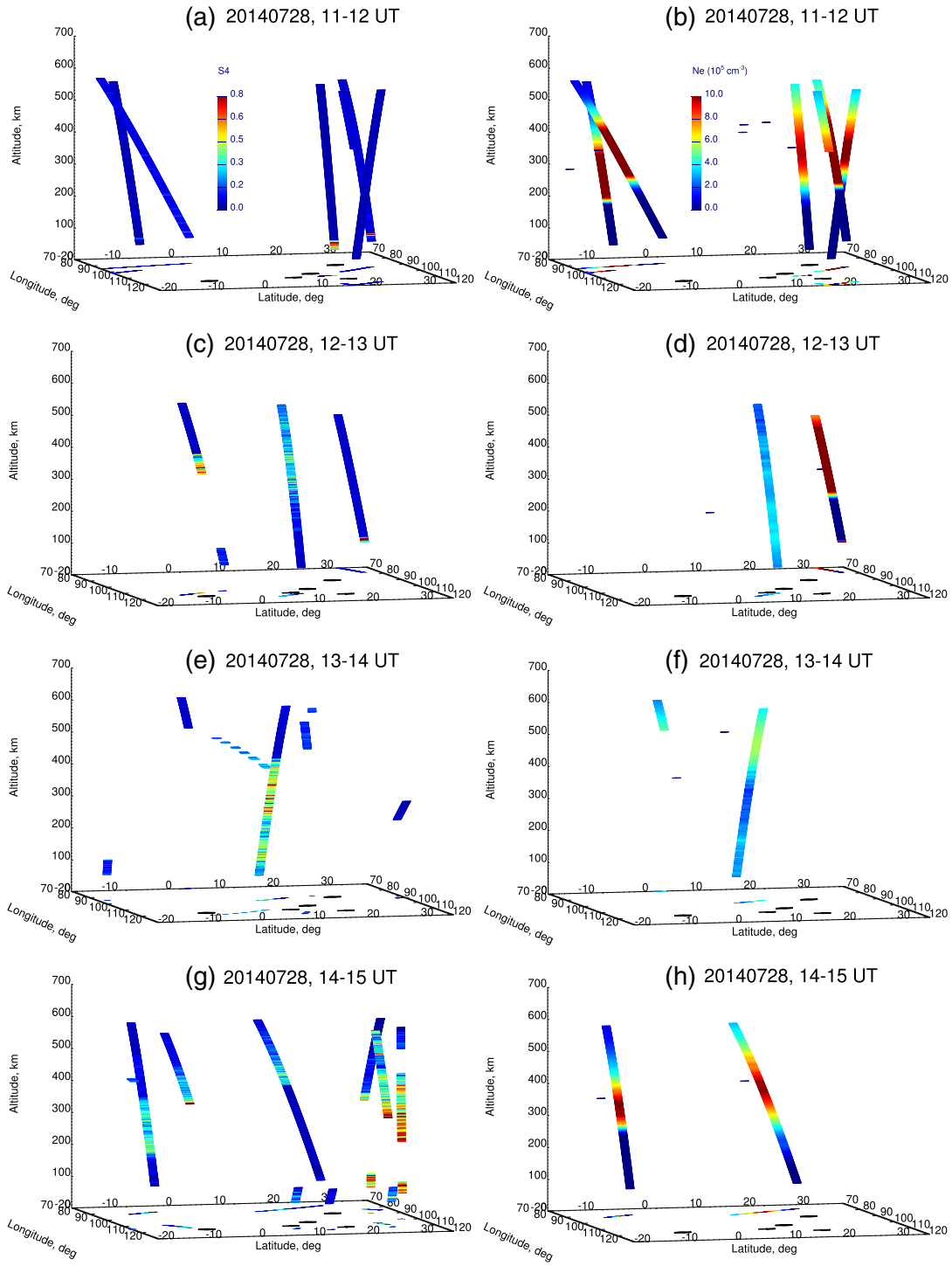

Fig. 4 Altitude - latitude - longitude plots restricted to the red rectangle in Fig. 2, showing the tangent point locations of the RO events that sampled the ionosphere each hour from 11 UT (top row) until 15 UT (bottom row) on 28 July 2014. The tangent points (and their respective projections in the latitude-longitude plane) in the left and right columns are colored according to the measured S4 index and electron density, respectively. The black dashes in the altitude-latitude plane in the right column show the peak electron density altitudes measured for each RO event. The black symbols in the latitude-longitude plane indicate the station locations, as in Fig. 2. Note that RO profiles are plotted from 80 to 600 km altitude in this figure **a** 20140728, 11-12 UT, **b** 20140728, 11-12 UT, **c** 20140728, 12-13 UT, **d** 20140728, 12-13 UT, **e** 20140728, 13-14 UT, **f** 20140728, 13-14 UT, **g** 20140728, 14-15 UT, **h** 20140728, 14-15 UT

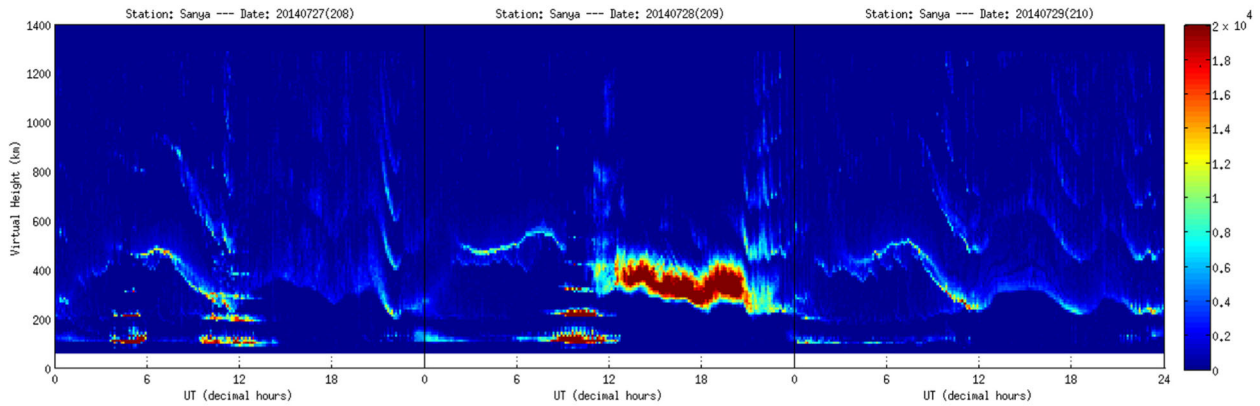

Fig. 5 Range-time-intensity-style plot of ionospheric echoes received from the Sanya ionosonde during 27–29 July 2014. Ionograms collected every 15 min were used to generate this figure. The color scale indicates the number of echoes across all sounding frequencies

to the significantly enhanced PRE on the same evening that would have significantly enhanced the R-T growth conditions.

During this time of year in the Southeast Asian longitude sector, the PRE should be weak due to the misalignment of the local magnetic field with the solar terminator (e.g., Abdu et al. 1981; Tsunoda 1985). This misalignment decreases the longitudinal conductivity gradient in the E layer, which effectively suppresses the polarization electric field strength that causes the PRE shortly after sunset.

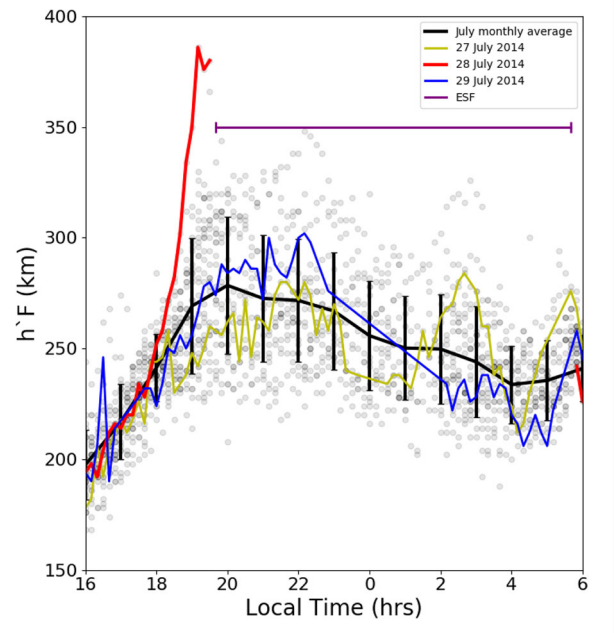

Fig. 6 The hourly average of h'F versus local time throughout July 2014 (black, error bars indicate ± 1 standard deviation) and the h'F versus local time for 27 (yellow), 28 (red), and 29 (blue) July 2014, as measured by the BCL ionosonde. The horizontal bar indicates the presence of spread F on 28 July

This characterization of the equatorial ionospheric electrodynamics is well supported by the average h'F variation throughout July in Fig. 6. However, the PRE on 28 July is a clear exception to this explanation and indicates that the ionospheric electrodynamics were significantly modified on this evening. As such, the key to understanding the causal mechanism(s) behind the 28 July unseasonal EPB event lies in exploring the reason(s) how the background equatorial electrodynamics were modified to produce such a strong PRE.

A complicated relationship between the PRE strength and the prevailing geomagnetic activity conditions has been the subject of significant research attention in recent years (see review by Abdu (2012)). The connection between geomagnetic activity (i.e., forcing from above) and the PRE strength can be placed into two categories: eastward electric fields that enhance the PRE (upward $\vec{E} \times \vec{B}$ drift) and westward electric fields that suppress the PRE (downward $\vec{E} \times \vec{B}$ drift). One source of the westward electric fields is the so-called "over-shielding" electric field (Kelley et al. 1979; Abdu 2012), which penetrates from the high latitudes to the magnetic equator following a sudden northward turning of the interplanetary magnetic field (IMF). Another source of westward electric fields is the disturbance dynamo, which is caused by a westward neutral wind enhancement from mid-latitudes to the equator that occurs a few hours following an increase of geomagnetic activity (Blanc and Richmond 1980). The eastward penetration electric field that enhances the PRE is known as the "under-shielding" electric field (or the "prompt-penetration electric field," PPEF) that follows a sudden southward turning of the IMF (e.g., Huang et al. 2005; Tulasi Ram et al. 2008).

If geomagnetic activity was responsible for the enhanced PRE in Southeast Asia on this particular evening, then the "under-shielding" eastward-directed electric field (i.e., PPEF) is the only possible candidate

because both disturbance dynamo and over-shielding electric fields are westward after sunset. Figure 7 shows a geomagnetic activity summary throughout the month of July 2014. Shown are the SYM-H index, the solar wind dynamic pressure, the solar wind speed, the AE index, and the interplanetary electric field (IEF); the solar wind parameters measured at the L1 point have been shifted in time to the bow shock. The month of July was very geomagnetically quiet. The SYM-H index was consistently above −35 nT, the AE index was mostly below 500 nT, and the magnitude of the IEF was primarily below 2 mV/m. The most notable event was the solar wind shock that preceded a corotation interaction region (CIR) on 14 July. Another CIR arrived on 28 July, but the magnitudes of the solar wind shock and the solar wind speed were significantly smaller than the 14 July event.

Figure 8 shows the geomagnetic activity summary for 28 July 2014. A close observation of the solar wind data reveals that a few small solar wind shocks arrived on the day of interest that were associated with the CIR. The largest shock was followed by some minor auroral activity, as indicated by the AE index. A PPEF can be spotted in the IEF data as a positive turning (indicating a southward IMF Bz turning). PPEFs are also known to penetrate to the equator almost instantaneously and last for up to a few hours (i.e., the time it takes for the shielding electric field within the magnetosphere to build up and counter the PPEF from the solar wind). Thus, at 4 UT, the positive IEF indicates the presence of a small-magnitude PPEF, but this PPEF occurs too early to have caused the PRE enhancement over the Southeast Asian sector, which occurred at 11–12 UT. Further, the IEF is negative at the time of the PRE. Therefore, the possibility that the enhanced PRE on the evening of 28 July 2014 was caused by PPEFs, or any other forcing from above for that matter, can be rather confidently ruled out.

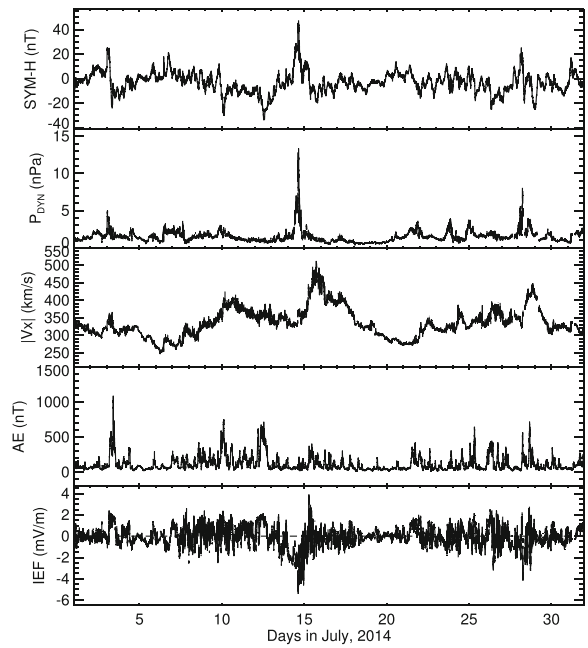

Fig. 7 Overview of solar wind and geomagnetic activity throughout the month of July 2014. The top panel shows the SYM-H index, the second panel shows the solar wind dynamic pressure, the third shows the solar wind speed, the fourth panel shows the AE index, and the fifth shows the interplanetary electric field (IEF). Note that the solar wind dynamic pressure and the IEF have been propagated in time to the magnetopause location

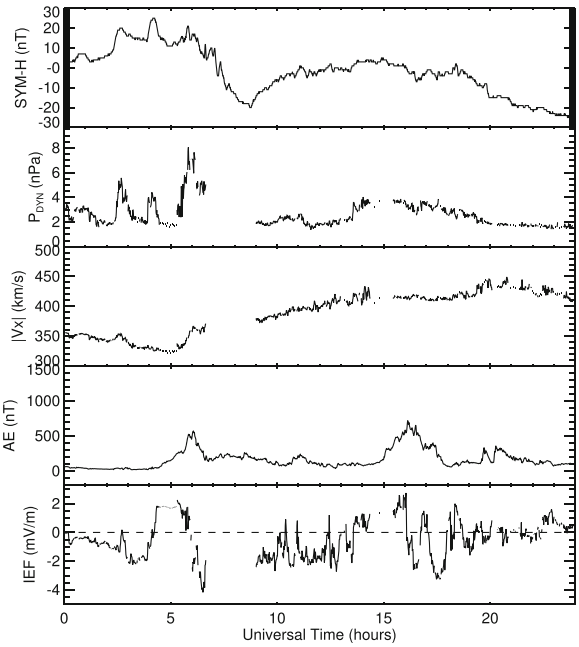

Fig. 8 The same as Fig. 7, but zoomed in on July 28 2014

Recent research has shown that the vertical plasma drift in the F region above the equator can also be influenced by lower atmospheric variability in the form of tides and planetary waves (e.g., Abdu et al. 2006, 2015; Maute et al. 2014); i.e., forcing from below. Atmospheric gravity waves from the troposphere are also suspected to influence the F-region vertical plasma drift (Li et al. 2016) and play a role in the seeding and development of EPBs (e.g., McClure et al. 1998; Tsunoda 2010a, b); atmospheric gravity waves therefore represent another form of forcing from below. One would expect that atmospheric gravity waves that seed EPBs would originate from a local source, whereas tides or planetary waves would be expected to exhibit larger scale, perhaps even global, effects. The analysis of GPS RO data in Fig. 2 and ground-based VHF scintillation data in Fig. 3, which show a lack of EPBs in both the African and Pacific sectors on the day of the EPB event over Southeast Asia, indicates that perhaps a global-scale variation of the PRE occurred.

Although, if tidal or planetary wave activity is responsible for such large-scale PRE variations, it is not entirely clear why the PRE would be enhanced above Southeast Asia and suppressed over the Pacific and Africa on the same day. Further, one would expect recurrent EPB events throughout July if planetary wave activity was the root cause of the PRE enhancement, but recurrent EPB events are not observed in Fig. 1. It is also possible that longitudinal structuring of the ionosphere could be playing a role in generating this large PRE over Southeast Asia, but the relationship between longitudinal structure and the day-to-day EPB variability is still an open question (Saito and Maruyama 2007). More evidence and investigation of this unseasonal EPB event is needed in order to properly investigate whether or not lower atmospheric forcing is responsible, and this is the topic of a companion paper (Ajith et al. 2017).

Conclusions

Understanding the daily variability in the occurrence of EPBs is an ongoing challenge. In this study, an unseasonal EPB event over the Southeast Asian region on 28 July 2014 was examined using a collection of ground-based and space-based data. Ionosonde data revealed the presence of an abnormally strong PRE in the upward plasma drift over Southeast Asia, which created favorable conditions for the R-T plasma instability to operate on this evening. While the connection between the enhanced PRE and the presence of EPBs is clear from this analysis, the exact cause of the strong PRE has not yet been determined. Penetration electric fields from the solar wind-magnetosphere interactions were considered as potential sources, but they were effectively ruled out using solar wind data. GPS RO data revealed that the presence of EPBs over Southeast Asia coincided with the suppression of EPBs in both the African and Pacific longitude sectors, suggesting that a large-scale phenomenon may be responsible. This observation, in combination with the lack of penetration electric fields, indicates that perhaps tidal/planetary wave activity from the lower atmosphere could potentially be the source of the enhanced PRE and the resulting EPBs during an off-peak EPB season. Future research efforts aimed at understanding all of the driving mechanisms of unseasonal EPB events are strongly encouraged.

Acknowledgements

This publication makes use of data from ionosonde stations, owned by Institute of Geology and Geophysics, Chinese Academy of Sciences (IGGCAS) and supported in part by Solar-Terrestrial Environment Research Network of CAS and Meridian Project of China. The authors would like to thank B. W. Reinisch of the University of Massachusetts Lowell for making the GIRO ionogram images available online. The COSMIC Radio Occultation data was collected from UCAR's CDAAC website; http://cdaac-www.cosmic.ucar.edu/. The geophysical data was obtained from NASA's Space Physics Data Facility; https://omniweb.gsfc.nasa.gov/.

Funding

This research was supported by the Australian Research Council Linkage grant (project LP160100561) and the Victorian Postdoctoral Research Fellowship awarded to BAC.

Authors' contributions

BAC led the research presented in this paper. STR, EY, RP, JR, RN, JC, MT, and KZ assisted with the data analysis and interpretation. KG, RC, and TY provided and assisted in the quality control of SCINDA and SEALION data, respectively. All authors read and approved the final manuscript.

Competing interests

The authors declare that they have no competing interest.

Publisher's Note

Author details

[1] SPACE Research Centre, RMIT University, Melbourne, Victoria, Australia. [2] Indian Institute of Geomagnetism, Mumbai, India. [3] Institute for Scientific Research, Boston College, Boston, MA, USA. [4] Space Vehicles Directorate, Air Force Research Laboratory, Kirtland AFB, NM, USA. [5] Space Weather Services, Bureau of Meteorology, Sydney, New South Wales, Australia. [6] National Institute of Information and Communications Technology, Tokyo, Japan.

Received: 4 May 2017 Accepted: 8 January 2018
Published online: 13 February 2018

References

Aarons J (1993) The longitudinal morphology of equatorial F-layer irregularities relevant to their occurrence. Space Sci Rev 63:209–243

Abdu MA, Bittencourt JA, Batista IS (1981) Magnetic declination control of the equatorial F region dynamo electric field development and spread F. J Geophys Res 86:11443–11446

Abdu MA, Batista PP, Batista IS, Brum CGM, Carrasco AJ, Reinisch BW (2006) Planetary wave oscillations in mesospheric winds, equatorial evening prereversal electric field and spread F. Geophys Res Lett 33(7). https://doi.org/10.1029/2005GL024837.L07107

Abdu MA (2012) Equatorial spread F/plasma bubble irregularities under storm time disturbance electric fields. J Atmos Sol Terr Phys 75-76:44–56

Abdu MA, Brum CG, Batista PP, Gurubaran S, Pancheva D, Bageston JV, Batista IS, Takahashi H (2015) Fast and ultrafast Kelvin wave modulations of the equatorial evening F region vertical drift and spread F development. Earth, Planets and Space 67(1):1. https://doi.org/10.1186/s40623-014-0143-5

Ajith KK, Tulasi Ram S, Carter BA, Yamamoto M, Gurubaran S, Sripathi S, Hozumi K, Groves K, Caton RG (2017) Unseasonal development of F-region irregularities over Southeast Asia on 28 july 2014: 2. forcing from below? Prog Earth Planet Sci. https://doi.org/PEPS-D-17-00070

Anderson DN, Reinisch B, Valladares C, Chau J, Veliz O (2004) Forecasting the occurrence of ionospheric scintillation activity in the equatorial ionosphere on a day-to-day basis. J Atmos Sol Terr Phys 66:1567–1572

Anderson DN, Redmon RJ (2017) Forecasting scintillation activity and equatorial spread-F. Space Weather 15:495–502. https://doi.org/10.1002/2016SW001554. 2016SW001554

Anthes RA (2011) Exploring Earth's atmosphere with radio occultation: contributions to weather, climate and space weather. Atmos Meas Tech 4(6):1077–1103. https://doi.org/10.5194/amt-4-1077-2011

Arras C, Wickert J, Beyerle G, Heise S, Schmidt T, Jacobi C (2008) A global climatology of ionospheric irregularities derived from GPS radio occultation. Geophys Res Lett 35. https://doi.org/10.1029/2008GL034158. L14809

Blanc M, Richmond AD (1980) The ionospheric disturbance dynamo. J Geophys Res 85:1669–1686. https://doi.org/10.1029/JA085iA04p01669

Brahmanandam PS, Uma G, Liu JY, Chu YH, Devi NSMPL, Kakinami Y (2012) Global S4 index variations observed using FORMOSAT-3/COSMIC GPS RO technique during a solar minimum year. J Geophys Res 117. https://doi.org/10.1029/2012JA017966. A09322

Burke WJ, Gentile LC, Huang CY, Valladres CE, Su SY (2004) Longitudinal variability of equatorial plasma bubbles observed by DMSP and ROCSAT-1. J Geophys Res 109. https://doi.org/10.1029/2004JA010583. A12301

Carter BA, Zhang K, Norman R, Kumar VV, Kumar S (2013) On the occurrence of equatorial F-region irregularities during solar minimum using radio occultation measurements. J Geophys Res 118:892–904. https://doi.org/10.1002/jgra.50089

Carter BA, Retterer JM, Yizengaw E, Groves K, Caton R, McNamara L, Bridgwood C, Francis M, Terkildsen M, Norman R, Zhang K (2014a) Geomagnetic control of equatorial plasma bubble activity modeled by the TIEGCM with Kp. Geophys Res Lett 41:5331–5339. https://doi.org/10.1002/2014GL060953

Carter BA, Retterer JM, Yizengaw E, Wiens K, Wing S, Groves K, Caton R, Bridgwood C, Francis M, Terkildsen M, Norman R, Zhang K (2014b) Using solar wind data to predict daily GPS scintillation occurrence in the African and Asian low-latitude regions. Geophys Res Lett 41(23):8176–8184. https://dx.doi.org/10.1002/2014GL062203

Carter BA, Yizengaw E, Retterer JM, Francis M, Terkildsen M, Marshall R, Norman R, Zhang K (2014c) An analysis of the quiet-time day-to-day variability in the formation of post-sunset equatorial plasma bubbles in the Southeast Asian region. J Geophys Res 119:3206–3223. https://doi.org/10.1002/2013JA019570

Carter BA, Yizengaw E, Pradipta R, Retterer JM, Groves K, Valladares C, Caton R, Bridgwood C, Norman R, Zhang K (2016) Global equatorial plasma bubble occurrence during the 2015 St. Patrick's Day storm. J Geophys Res Space Phys 121(1):894–905. https://doi.org/10.1002/2015JA022194

Chu YH, Wang CY, Wu KH, Chen KT, Tzeng KJ, Su CL, Feng W, Plane JMC (2014) Morphology of sporadic E layer retrieved from COSMIC GPS radio occultation measurements: wind shear theory examination. J Geophys Res Space Phys 119(3):2117–2136. https://doi.org/10.1002/2013JA019437

Dao E, Kelley MC, Roddy P, Retterer J, Ballenthin JO, de La Beaujardiere O, Su Y-J (2011) Longitudinal and seasonal dependence of nighttime equatorial plasma density irregularities during solar minimum detected on the C/NOFS satellite. Geophys Res Lett 38. https://doi.org/10.1029/2011GL047046

Dymond KF (2012) Global observations of L band scintillation at solar minimum made by COSMIC. Radio Sci 47. https://doi.org/10.1029/2011RS004931. RS0L18

Groves KM, Basu S, Weber EJ, Smitham M, Kuenzler H, Valladares CE, Sheehan R, MacKenzie E, Secan JA, Ning P, McNeill WJ, Moonan DW, Kendra MJ (1997) Equatorial scintillation and systems support. Radio Sci 32:2047–2064. https://doi.org/10.1029/97RS00836

Huang CY, Burke WJ, Machuzak JS, Gentile LC, Sultan PJ (2002) Equatorial plasma bubbles observed by DMSP satellites during a full solar cycle: toward a global climatology. J Geophys Res 107. https://doi.org/10.1029/2002JA009452. 1434

Huang C-M, Richmond AD, Chen M-Q (2005) Theoretical effects of geomagnetic activity on low-latitude ionospheric electric fields. J Geophys Res 110. https://doi.org/10.1029/2004JA010994. A05312

Huang C-S, Hairston MR (2015) The postsunset vertical plasma drift and its effects on the generation of equatorial plasma bubbles observed by the C/NOFS satellite. J Geophys Res Space Phys 120(3):2263–2275. https://doi.org/10.1002/2014JA020735. 2014JA020735

Kelley MC, Fejer BG, Gonzales CA (1979) An explanation for anomalous equatorial ionospheric electric fields associated with a northward turning of the interplanetary magnetic field. Geophys Res Lett 6(4):301–304. https://doi.org/10.1029/GL006i004p00301

Kelley MC, Retterer J (2008) First successful prediction of a convective equatorial ionospheric storm using solar wind parameters. Space Weather 8. https://doi.org/10.1029/2007SW000381. S08003

Kelley MC, Makela JJ, de La Beaujardiére O, Retterer J (2011) Convective ionospheric storms: a review. Rev Geophys 49. https://doi.org/10.1029/2010RG000340. RG2003

Li G, Ning B, Abdu MA, Yue X, Liu L, Wan W, Hu L (2011) On the occurrence of postmidnight equatorial F region irregularities during the June solstice. J Geophys Res Space Phys 116(A4):04318. https://doi.org/10.1029/2010JA016056

Li G, Otsuka Y, Ning B, Abdu MA, Yamamoto M, Wan W, Liu L, Abadi P (2016) Enhanced ionospheric plasma bubble generation in more active ITCZ. Geophys Res Lett 43(6):2389–2395. https://doi.org/10.1002/2016GL068145. 2016GL068145

Maruyama T, Kawamura M, Saito S, Nozaki K, Kato H, Hemmakorn N, Boonchuk T, Komolmis T, Ha Duyen C (2007) Low latitude ionosphere-thermosphere dynamics studies with inosonde chain in Southeast Asia. Ann Geophys 25(7):1569–1577. https://doi.org/10.5194/angeo-25-1569-2007

Maute A, Hagan ME, Richmond AD, Roble RG (2014) TIME-GCM study of the ionospheric equatorial vertical drift changes during the 2006 stratospheric sudden warming. J Geophys Res Space Phys 119(2):1287–1305. https://doi.org/10.1002/2013JA019490

McClure JP, Singh S, Bamgboye DK, Johnson FS, Kil H (1998) Occurrence of equatorial F region irregularities: evidence for tropospheric seeding. J Geophys Res 103:29119–29135

Nishioka M, Saito A, Tsugawa T (2008) Occurrence characteristics of plasma bubble derived from global ground-based GPS receiver networks. J Geophys Res 113. https://doi.org/10.1029/2007JA012605. A05301

Pi X, Mannucci AJ, Lindqwister UJ, Ho CM (1997) Monitoring of global ionospheric irregularities using the Worldwide GPS Network. Geophys Res Lett 24(18):2283–2286. https://doi.org/10.1029/97GL02273

Redmon RJ, Anderson D, Caton R, Bullett T (2010) A Forecasting Ionospheric Real-time Scintillation Tool (FIRST). Space Weather 8. https://doi.org/10.1029/2010SW000582. S12003

Reinisch BW, Galkin IA (2011) Global Ionospheric Radio Observatory (GIRO). Earth, Planets and Space 63(4):377–381. https://doi.org/10.5047/eps.2011.03.001

Retterer JM, Roddy P (2014) Faith in a seed: on the origins of equatorial plasma bubbles. Annales Geophysicae 32(5):485–498. https://doi.org/10.5194/angeo-32-485-2014, https://www.ann-geophys.net/32/485/2014/

Retterer J (2005) Physics-based forecasts of equatorial radio scintillation for the Communication and Navigation Outage Forecasting System (C/NOFS). Space Weather 3. https://doi.org/10.1029/2005SW000146. S12C03

Retterer J, Decker DT, Borer WS, R E Daniell J, Fejer BG (2005) Assimilative modeling of the equatorial ionosphere for scintillation forecasting: modeling with vertical drifts. J Geophys Res 110. https://doi.org/10.1029/2002JA009613. A11307

Retterer JM, Gentile LC (2009) Modeling the climatology of equatorial plasma bubbles observed by DMSP. Radio Sci 44. https://doi.org/10.1029/2008RS004057. RS0A31

Rocken C, Kuo Y-H, Schreiner W, Hunt D, Sokolovskiy S, McCormick C (2000) COSMIC system description. Terr Atmos Oceanic Sci 11:21–52

Saito S, Maruyama T (2007) Large-scale longitudinal variation in ionospheric height and equatorial spread F occurrences observed by ionosondes. Geophys Res Lett 34(16). https://doi.org/10.1029/2007GL030618

Scherliess L, Fejer BG (1999) Radar and satellite global equatorial F region vertical drift model. J Geophys Res 104:6829–6842

Su S-Y, Chao CK, Liu CH (2008) On monthly/seasonal/longitudinal variations of equatorial irregularity occurrences and their relationship with the postsunset vertical drift velocities. J Geophys Res 113. https://doi.org/10.1029/2007JA012809. A05307

Sultan PJ (1996) Linear theory and modeling of the Rayleigh-Taylor instability leading to the occurrence of equatorial spread F. J Geophys Res 101:26875–26891

Tulasi Ram S, Rama Rao PVS, Niranjan K, Prasad DSVVD, Sridharan R, Devasia CV, Ravindran S (2006) The role of post-sunset vertical drifts at the equator in predicting the onset of VHF scintillations during high and low sunspot activity years. Ann Geophys 24(6):1609–1616. https://doi.org/10.5194/angeo-24-1609-2006

Tulasi Ram S, Rama Rao PVS, Prasad DSVVD, Niranjan K, Gopi Krishna S, Sridharan R, Ravindran S (2008) Local time dependent response of postsunset ESF during geomagnetic storms. J Geophys Res 113. https://doi.org/10.1029/2007JA012922. A07310

Tsunoda RT (1985) Control of the seasonal and longitudinal occurrence of equatorial scintillations by the longitudinal gradient in integrated E region Pedersen conductivity. J Geophys Res 90:447–456

Tsunoda RT (2010a) On equatorial spread F: establishing a seeding hypothesis. J Geophys Res 115. https://doi.org/10.1029/2010JA015564. A12303

Tsunoda RT (2010b) On seeding equatorial spread F during solstices. Geophys Res Lett 37. https://doi.org/10.1029/2010GL042576. L05102

Whalen JA (2009) The linear dependence of GHz scintillation on electron density observed in the equatorial anomaly. Ann Geophys 27:1755–1761. https://doi.org/10.5194/angeo-27-1755-2009

Wu DL, Ao CO, Hajj GA, de la Torre Juarez M, Mannucci AJ (2005) https://doi.org/10.1029/2004JA010701. A01306. J Geophys Res Space Phys 110(A1)
Xiong C, Stolle C, Lühr H (2016) The Swarm satellite loss of GPS signal and its relation to ionospheric plasma irregularities. Space Weather 14(8):563–577. https://doi.org/10.1002/2016SW001439. 2016SW001439
Yokoyama T, Yamamoto M, Otsuka Y, Nishioka M, Tsugawa T, Watanabe S, Pfaff RF (2011) On postmidnight low-latitude ionospheric irregularities during solar minimum: 1. Equatorial Atmosphere Radar and GPS-TEC observations in Indonesia. J Geophys Res Space Phys 116(A11):11325. https://doi.org/10.1029/2011JA016797
Yu X, Yue X, Zhen W, Xu J, Liu D, Guo S (2017) On the occurrence of F region irregularities over Haikou retrieved from COSMIC GPS radio occultation and ground-based ionospheric scintillation monitor observations. Radio Sci 52(1):34–48. https://doi.org/10.1002/2016RS006014